Experimental section

1.1 Chemicals and reagents

All chemicals were purchased directly to be used without further purification. Tungsten (VI) chloride (WCl_6, 99%, Macklin), Ruthenium chloride hydrate ($RuCl_3$, 99.95%, Aladdin), 1,10-Phenanthroline ($C_{12}H_8N_2$, 99%, Aladdin), D-(+)-Glucose monohydrate ($C_6H_{12}O_6 \cdot H_2O$, 98% Aladdin), Nickel nitrate hexahydrate ($Ni(NO_3)_2 \cdot 6H_2O$, 99%, Aladdin), Iron nitrate nonahydrate ($Fe(NO_3)_3 \cdot 9H_2O$, 98%, Aladdin), Urea ($(NH_2)_2CO$, 99%, Aladdin), platinum/carbon commercial catalyst (Pt/C, 20wt%, Aladdin), Potassium hydroxide (KOH, 99.99%, Aladdin), nickel foam (NF).

1.2 Synthesis of catalysts.

1.2.1 Synthesis of Ru-W_2N/WO_2 and W_2N/WO_2.

Ru-W_2N/WO_2 is typically prepared using the co-precipitation and calcination method. First, 0.013g $RuCl_3$、0.495g WCl_6、1g $C_{12}H_8N_2$ 和 1g $C_6H_{12}O_6$ are ultrasonically dissolved in 40 ml of deionized water in a beaker. The solution is continuously stirred for 2 hours to ensure thorough mixing. After the reaction is completed, the generated precipitate is separated from the mother liquor by centrifugation at a speed of 7000 r min^{-1} for 15 minutes. The precipitate is then washed with deionized water to remove the impurity ions adsorbed on the surface. After three repeated washings, the obtained precipitate is dried in a vacuum at 60 °C for 12 hours. Subsequently, the precipitate is placed in a tube furnace under an Ar atmosphere. It is heated from room temperature to 750 °C at a heating rate of 5 °C min^{-1} and then maintained at this temperature for 2 hours. After natural cooling, a black block-shaped sample of Ru-W_2N/WO_2 is obtained, which is ground for later use. The synthesis process of W_2N/WO_2 is similar to that of Ru-W_2N/WO_2, except that $RuCl_3$ is not introduced.

1.2.2 Synthesis of NiFe LDH.

First, a solution was prepared by dissolving 0.5 mmol of $Fe(NO_3)_3 \cdot 9H_2O$, 0.5 mmol of $Ni(NO_3)_2 \cdot 6H_2O$, and 5 mmol of $(NH_2)_2CO$ in 40 mmol of distilled water. Then, the above-mentioned solution and nickel foam were transferred into a polytetrafluoroethylene-coated autoclave and placed in a drying oven, and maintained at 120 °C for 12 hours. After the obtained

sample was rinsed with deionized water, it was dried to obtain the final sample.

1.3 Materials Characterization:

The crystal structure of the catalyst was characterized via powder X-ray diffraction. (XRD, Smart Lab, 3 kW) with a Cu Kα radiation (λ = 1.5408 Å) source in the 2θ range of 25-85°.Sample morphology and microstructure were determined by aberration-corrected transmission electron microscope （AC-TEM, Titan Themis G2）, field-emission scanning electron microscopy (SEM, Regulus8100) and transmission electron microscopy (TEM, HT7700). Surface elemental analysis was justified via x-ray photoelectron spectroscopy (XPS, Thermo Scientific ESCALAB 250Xi). The work function of all samples was measured by ultraviolet photoelectron spectroscopy (UPS, ThermoFisher Nexsa).

1.4 XAFS data processing

The X-ray absorption find structure spectra (Ru K-edge and W L_3-edge) were collected with Si (111) crystal monochromators at the BL14W1 beamlines at the Shanghai Synchrotron Radiation Facility (SSRF) (Shanghai, China), the data collection was carried out in transmission mode using ionization chamber for Ru foil, RuO_2, WO_2, WO_3 and W foil, and in fluorescence excitation mode using a Lytle detector for Ru-W_2N/WO_2-Ru, Ru- W_2N/WO_2-W and W_2N/WO_2-W. All spectra were collected in ambient conditions.

The XAFS data were processed according to the standard procedures using the Athena module implemented in the IFEFFIT software packages. The EXAFS spectra were obtained by subtracting the post-edge background from the overall absorption and then normalizing with respect to the edge-jump step. Subsequently, the χ(k) data of were Fourier transformed to real (R) space using a hanning windows (dk = 1.0 $Å^{-1}$) to separate the EXAFS contributions from different coordination shells. To obtain the quantitative structural parameters around central atoms, least-squares curve parameter fitting was performed using the ARTEMIS module of IFEFFIT software packages.

1.5 Electrochemical Measurements

Dispersing 5 mg catalyst into 20 μL Nafion solution and isopropanol solution (480 μL), and then sonicated for 30 minutes to form a uniform ink. Then, 20 μL ink is dropped onto a 1*0.8cm carbon paper (containing 0.2 mg of catalyst).

All electrochemical measurements were conducted using the electrochemical station (CHI 760E) in a standard three-electrode system at room temperature (~ 25 ℃). Prepared samples were applied as working electrodes. The Hg/HgO and a graphite rod were used as reference and counter electrodes, respectively. LSV was recorded in the range 0 to -0.4 V vs. RHE for HER with a scan rate of 5 mV s^{-1}. To estimate the H-desorption characteristics, different scan rates of 20, 40, 60 80, and 100 mV s^{-1} CV cycles were performed in the range 0 to 0.8 V vs. RHE. The electrochemical impedance spectroscopy (EIS) measurements were performed at a given potential in the frequency range of 10^5 Hz to 10^{-2} Hz. To evaluate stability, chronoamperometric measurement curves were carried out at a constant current density. All potential was calibrated to the reversible hydrogen electrode (vs. RHE) according to the formula (E vs. RHE= E vs. Hg/HgO +0.098V+0.059 pH). In-situ Raman measures: The in-situ electrolytic cell is composed of a working electrode, platinum wire as the counter electrode, and Hg/HgO as the reference electrode. The laser wavelength used for all Raman tests was 532 nm. The corresponding Raman curve is obtained by applying a voltage to achieve a stable current.

1.6 Computational details

The $W_2N(111)/WO_2(101)$ and Ru-$W_2N(111)/WO_2(101)$ surfaces were built, where the vacuum space along the z direction is set to be 20 Å, which is enough to avoid interaction between the two neighboring images. All atoms were relaxed adequately to remove the internal stress of systems. Then, the H, H_2O, H_2, H+H, OH+H were absorbed on the W or Ru site. All the spin-polarized first-principles calculations were performed via the Vienna ab initio simulation package (VASP).[1] The ion-electron interactions were described by the projector augmented wave (PAW) method, and the generalized gradient approximation (GGA) with the Perdew-Burke-Ernzerh of (PBE) was used to treat the interaction of electronic exchange-

correlation energy.[2-4] The Monkhorst-Pack k-point mesh of 7x7x1 was set for all systems. The cutoff energy for plane-wave is 700 eV. The convergence threshold is 10^{-5} eV and 1×10^{-3} eV/Å for energy and force, respectively. The van der Waals interaction was treated by Grimme scheme (DFT-D3).[5] All atoms were relaxed. The transition state was also considered for the step of *H+*H →*H_2, and *H+*H_2O→*H_2+*OH.

Adsorption energy ΔE of A groups on the surface of substrates was defined as [6]:

$$\Delta E = E_{*A} - (E_{*} + E_{A}) \quad (1)$$

where *A and * denote the adsorption of A groups on substrates and the bare substrates, EA denotes the energy of A groups.

Free energy change ΔG of the reaction was calculated as the difference between the free energies of the initial and final states as shown below [6]:

$$\Delta G = \Delta E + \Delta ZPE - T\Delta S \quad (2)$$

where ΔE is the energy change between the reactant and product obtained from DFT calculations; ΔZPE is the change of zero point energy; T and ΔS denote temperature and change of entropy, respectively. In here, T = 300 K was considered.

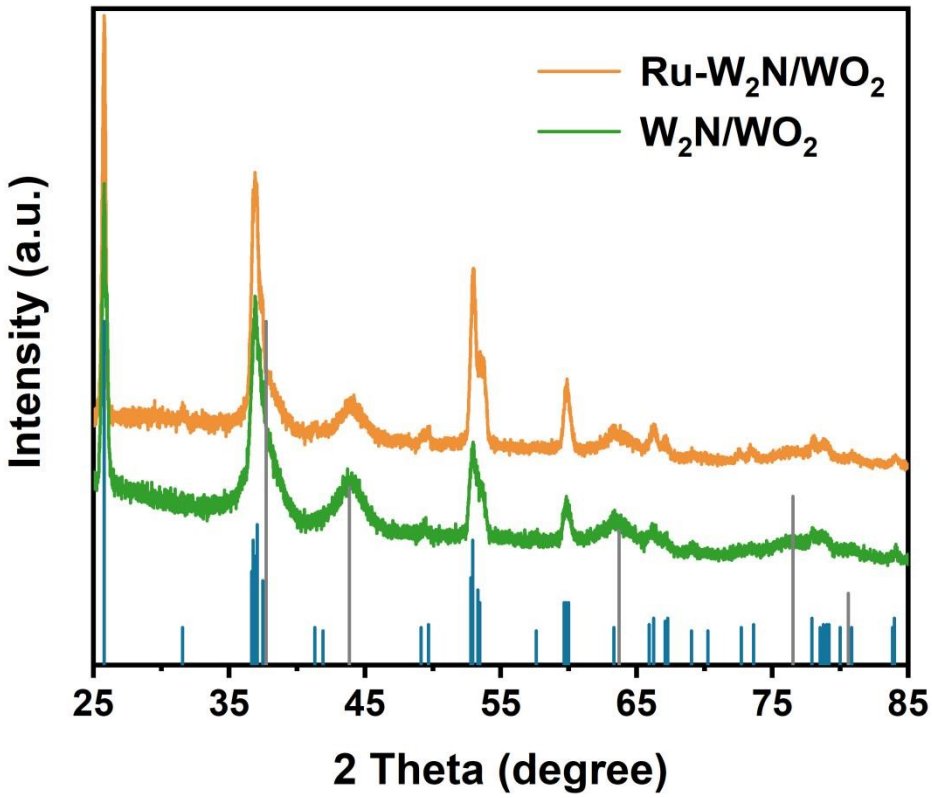

Figure S1. XRD patterns of prepared catalysts.

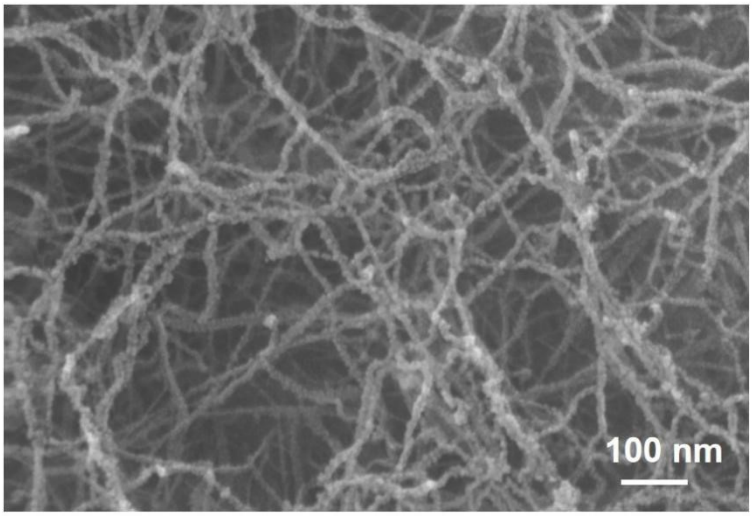

Figure S2. SEM image of Ru-W_2N/WO_2.

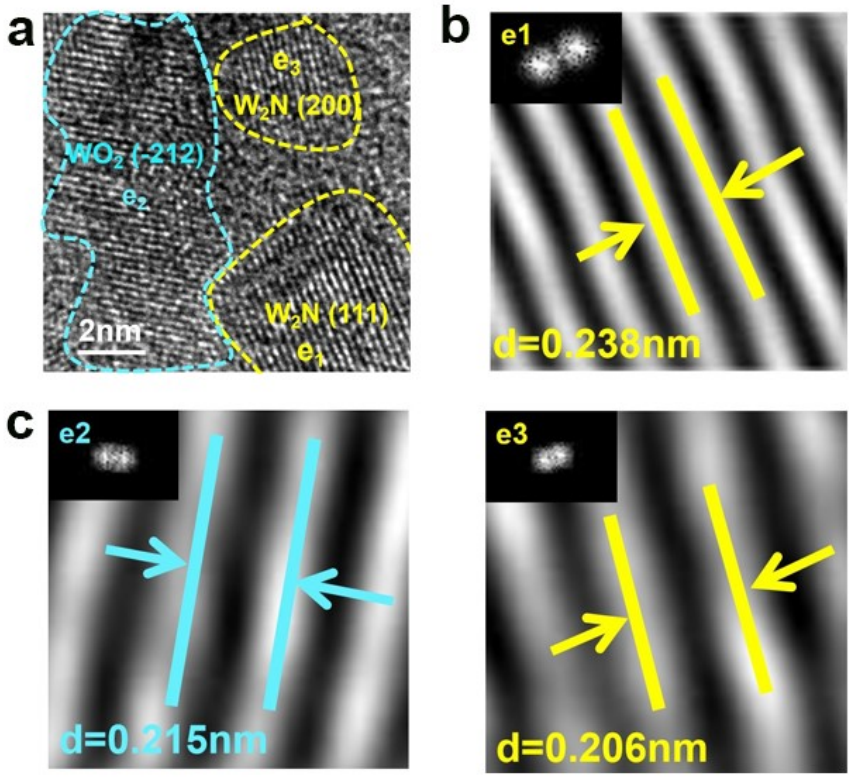

Figure S3. HRTEM images and the corresponding IFFT images of Ru-W_2N/WO_2.

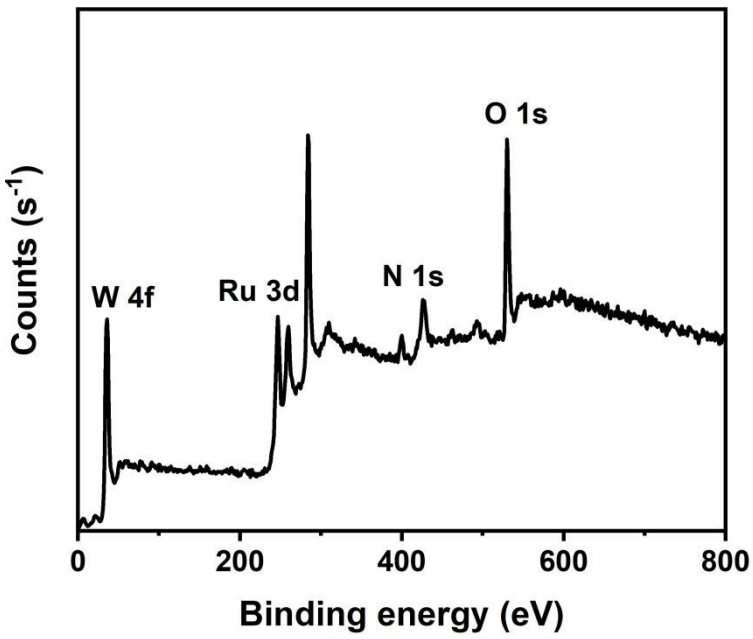

Figure S4. XPS survey spectrum of Ru-W_2N/WO_2.

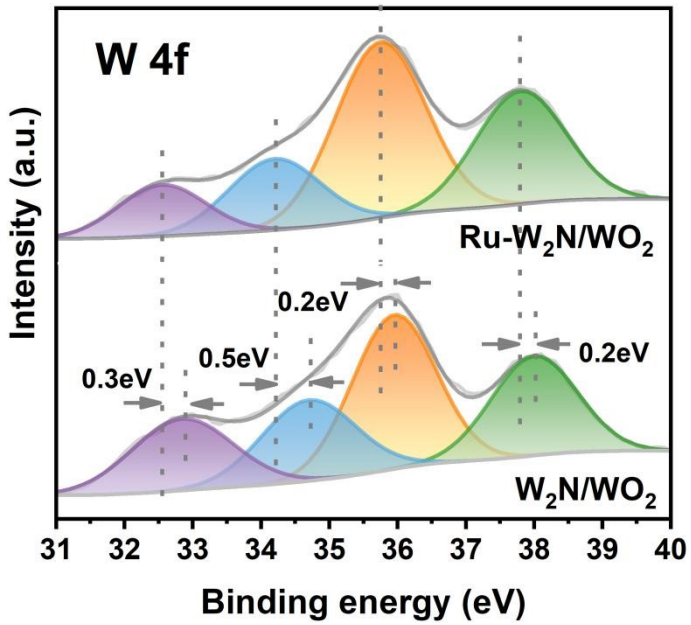

Figure S5. XPS W 4f spectra.

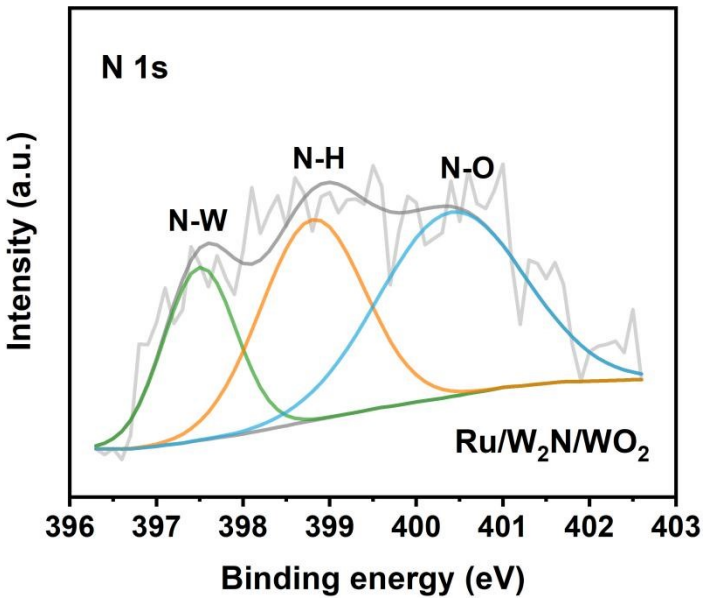

Figure S6. XPS N 1s spectra.

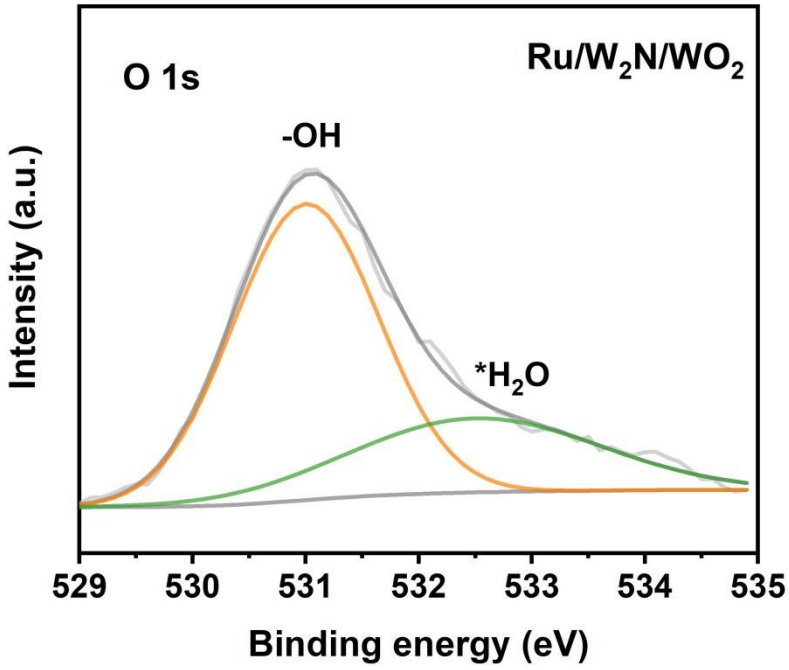

Figure S7. XPS O 1s spectra.

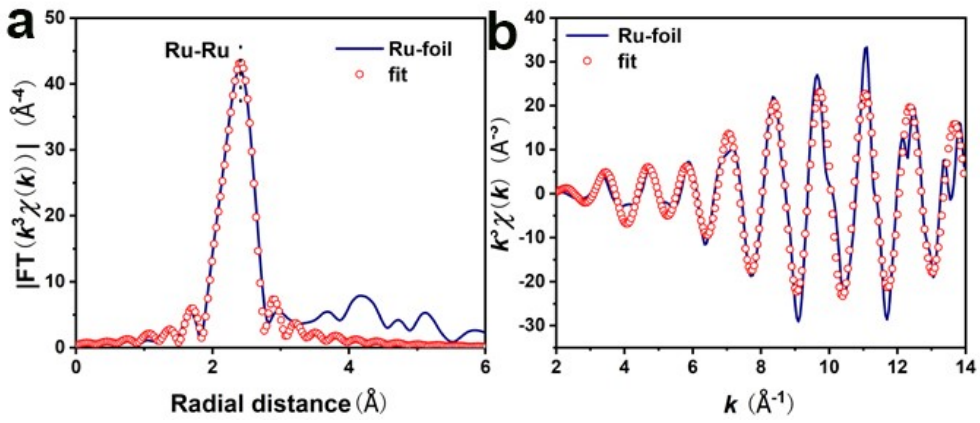

Figure S8. The Fourier transformed (FT)-EXAFS spectra of Ru species.

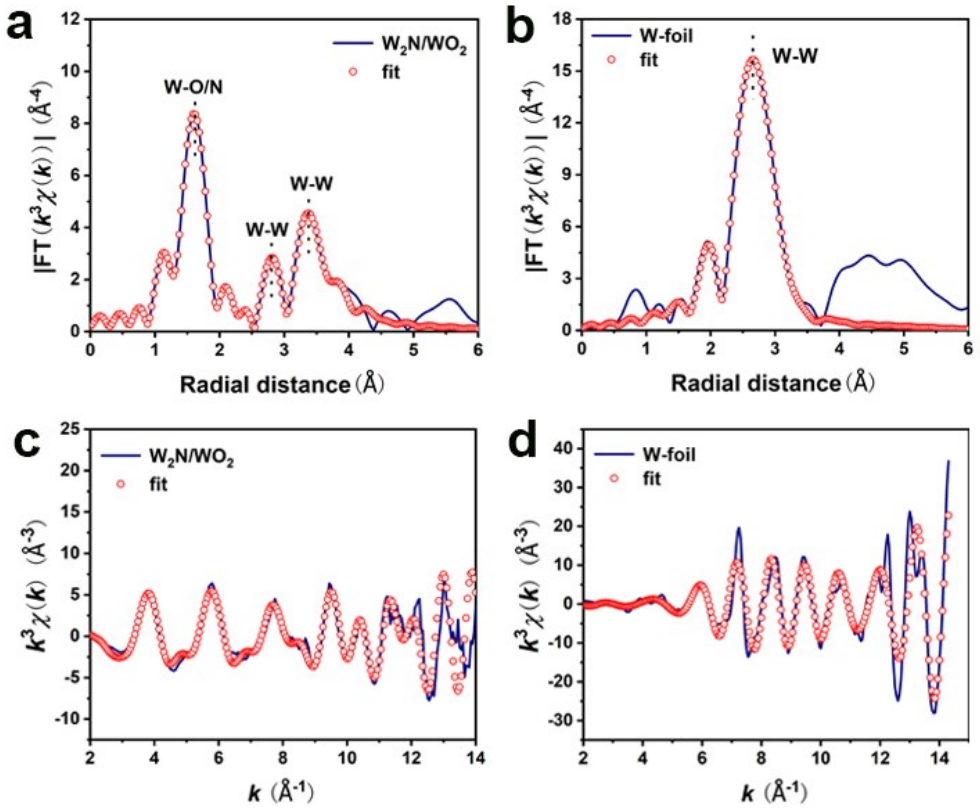

Figure S9. The Fourier transformed (FT)-EXAFS spectra of W species.

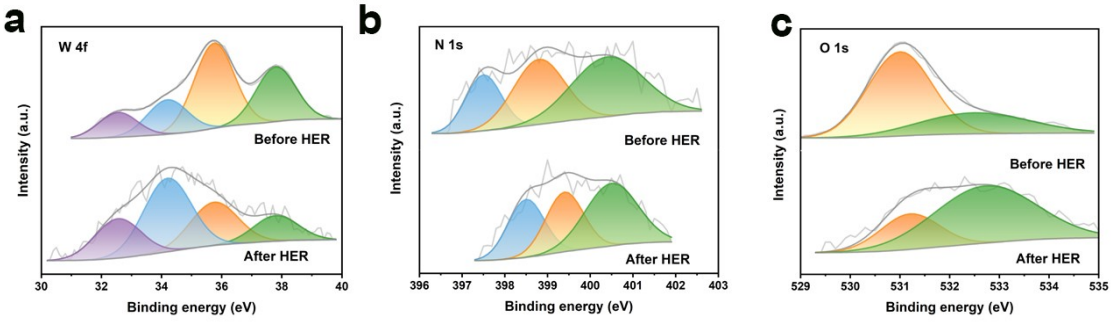

Figure S10. XPS spectra of Ru-W_2N/WO_2 before and after HER test.

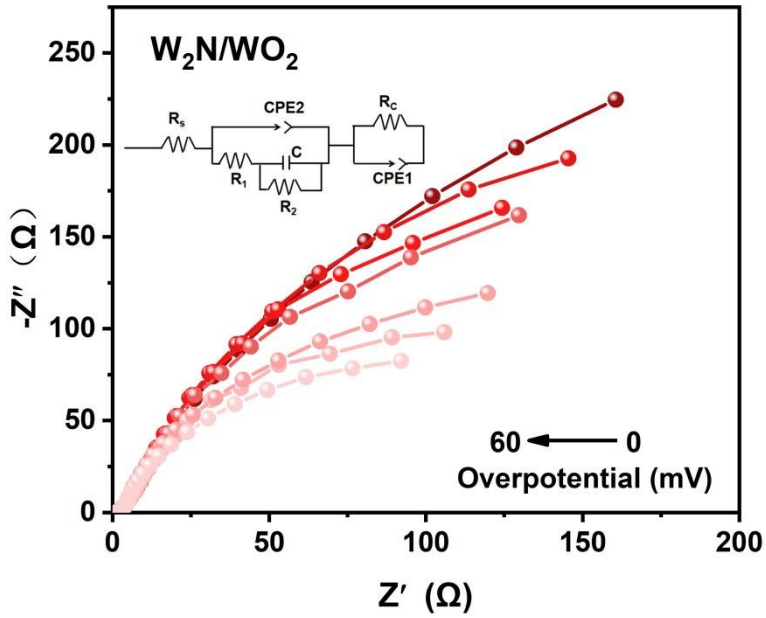

Figure S11. In situ EIS for HER process of W_2N/WO_2.

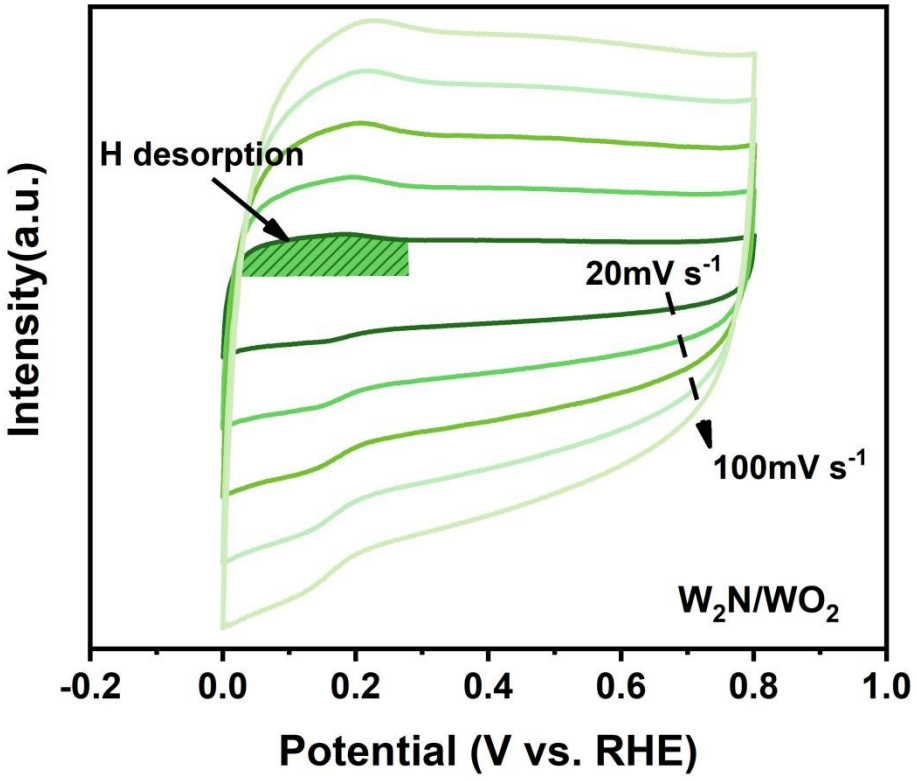

Figure S12.CV curves of W_2N/WO_2 with the scan rate from 20 to 100 mV s^{-1}.

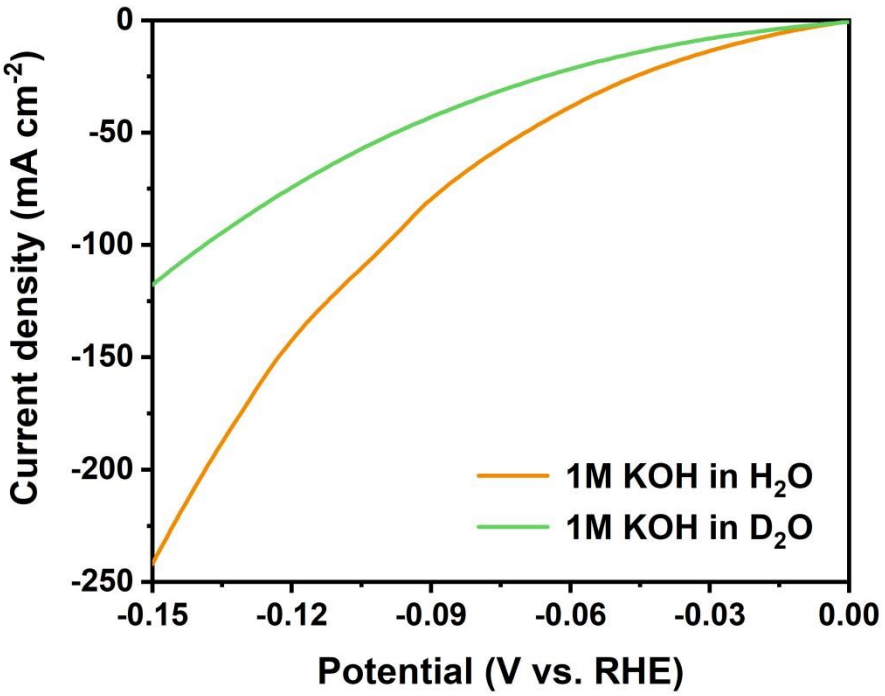

Figure S13. Polarization curves and KIE_s of Ru-W_2N/WO_2 in 1M KOH and KDH solution.

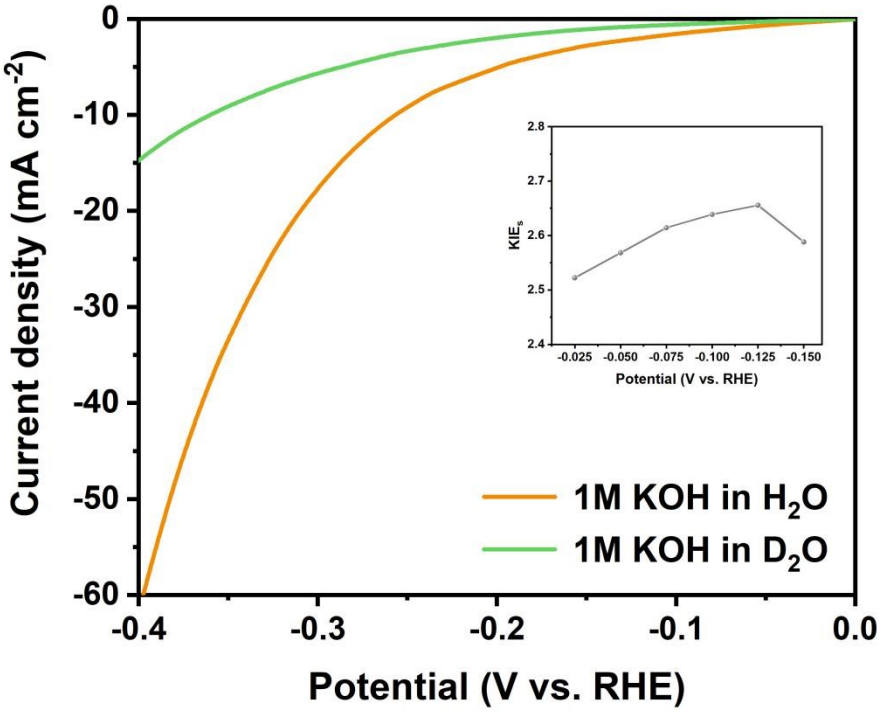

Figure S14. Polarization curves and KIE_s of W_2N/WO_2 in 1M KOH and KDH solution.

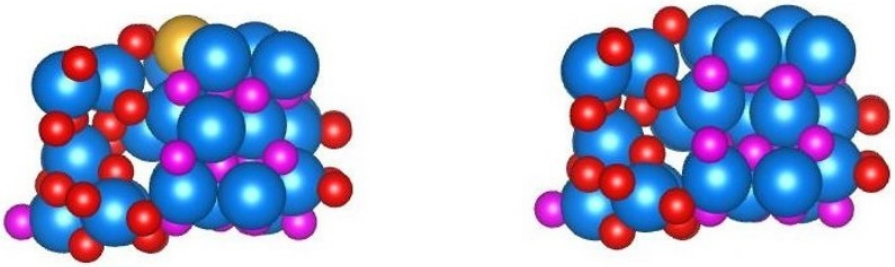

Figure S15. Optimized model of Ru-W_2N/WO_2.

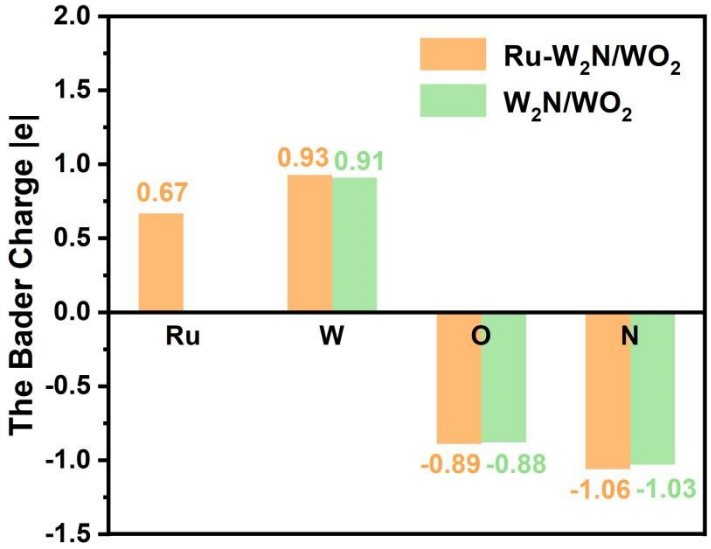

Figure S16. The Bader charge of Ru-W_2N/WO_2 and W_2N/WO_2 systems.

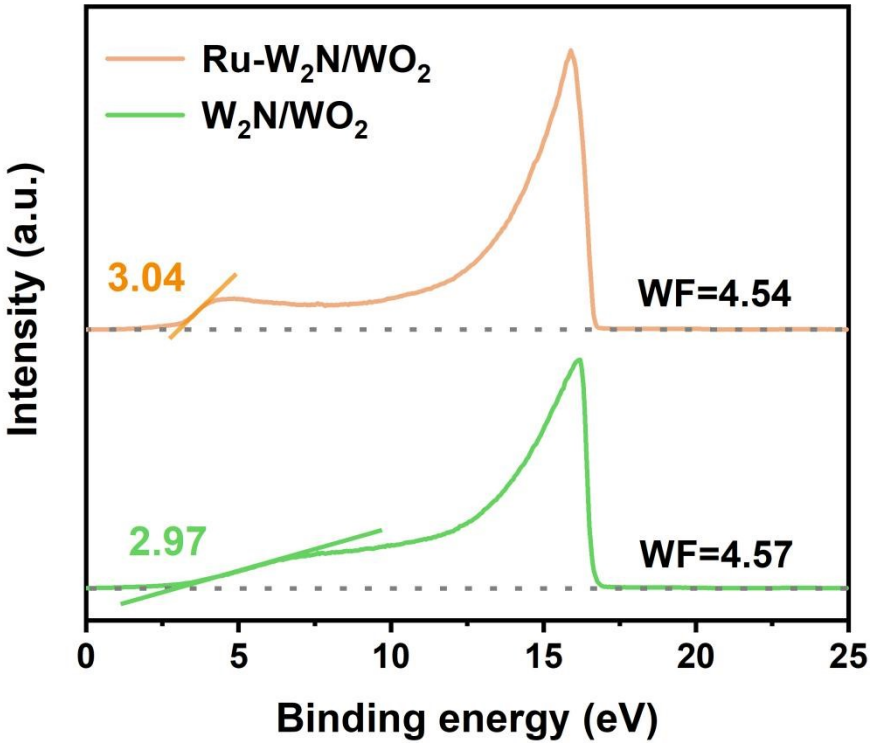

Figure S17.UPS spectra of Ru-W_2N/WO_2 and W_2N/WO_2.

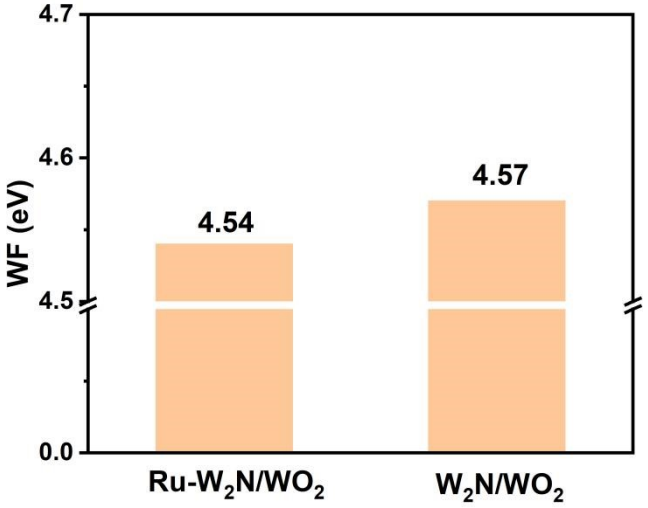

Figure S18. Work functions of Ru-W_2N/WO_2 and W_2N/WO_2.

Table1 ICP testing results of Ru-W_2N/WO_2.

Ru-W_2N/WO_2	W	Ru
Metal content(wt%)	68.15	0.86

Table2 EXAFS data fitting results of Samples of Ru species.

Sample	Path	R(Å)[b]
	Ru K-edge (S_0^2=0.910)	
Ru foil	Ru-Ru	2.675±0.003
	Ru-N	1.8932±0.008
Ru-W_2N/WO_2	Ru-O	2.082±0.019
	Ru-W	3.153±0.021

Table3 EXAFS data fitting results of Samples of W species.

Sample	Path	R(Å)[b]
	W L3-edge (S_0^2=0.840)	
W foil	W-W	2.733±0.004
	W-W	3.147±0.007
	W-N	2.054±0.020
	W-O	2.132±0.014
Ru-W_2N/WO_2	W-W	2.956±0.023
	W-Ru	3.156±0.018

		W-W	3.622±0.011
		W-N	2.010±0.011
		W-O	2.123±0.017
W_2N/WO_2		W-W	2.963±0.012
		W-W	3.570±0.019

Table4 EIS value in HER progress after fitting.

Catalysts	Potential (V vs.RHE)	R_s (Ω)	R_1 (Ω)	R_2 (Ω)	R_c (Ω)	C (F)
Ru-W_2N/WO_2	0	1.73	4.8	1.5	11.3	0.125
	0.01	1.65	4	1.44	10	0.151
	0.02	1.74	3.6	1.36	7	0.241
	0.03	1.77	3	1.24	5.2	0.335
	0.04	1.84	2	1.17	3.9	0.369
	0.05	1.74	1.61	1.06	3.86	0.4
	0.06	1.91	1.58	0.96	2.54	0.402
W_2N/WO_2	0	1.34	100	288	578	0.01
	0.01	1.28	97.2	224	382	0.032
	0.02	1.18	92	171	422	0.051
	0.03	1.15	89	121	372	0.061
	0.04	1.11	82	96	393	0.075
	0.05	1.08	78	78	238	0.091
	0.06	1.04	72	67	199	0.101

Table5. Performance of some reported materials and comparison with our work.

	HER	Tafel	Ref.
This work	22	29.1	
ECM@Ru	83	59	Advanced Energy Materials,2020, 10, 2000882.
Ni_5P_4 -Ru	54	52	Adv. Mater. 2020, 32, 1906972
LaRuSi	72	68	Angew. Chem. 2022, 134, e202206460
$LaNi_{0.5}Co_{0.5}Ru$	43	70	Angew. Chem. Int. Ed. 2024, 63, e202315340
Ru NPs/TiN	73	41.4	Nature Commun. 2024, 15, 50691
Ru-$NiPS_3$NSs	59	64	Nat Commun. 2024, 14, 6462
M-Co NPs@Ru	34	55	Small 2021, 17, 2105231.
Co-Ru DAS/Ru NPs/NC-4	41	45.16	Nano Res. 2024, 17, 3714
CoRu-BPDC	37	73.22	Small 2023, 19, 2301850.
Ru/NSCS	40	33.8	J. Mater. Chem. A, 2023,11, 14674
W_2CO_x-Ru/CC	52	26.82	Chemical Engineering Journal. 2023, 475, 146443.
Ru/S–Ni_2P	49	43.1	J. Mater. Chem. A, 2021,9, 15648
2.5%Ru–VS_2/CC	87	93	Nanoscale, 2024,16, 11250
Ru/Co_4N/NF	45	25	J. Mater. Chem. A, 2023,11, 22147
Co-Ru/NCN	70	64	Journal of Energy Chemistry. 2023, 87, 286
Ru-Co_2P@Ru-N-C	69	65	Adv. Funct. Mater. 2024, 34, 2316709.
Ru-MoCoP	55	67	Adv. Funct. Mater. 2024, 34, 2309330.
S-RuP@NPSC-900 p	92	90.23	Adv. Sci. 2020, 7, 2001526.
Ru-1T-MoS_2	81	54	J. Mater. Chem. A, 2022,10, 21013
$Ru_{0.10}$@2H-MoS_2	51	64.9	Applied Catalysis B: Environmental. 2021, 298, 120490
Ru-$NiCo_2S_4$	32	41.3	Adv. Funct. Mater. 2022, 32, 2109731.
Ru@NC (2 wt%)	26	36	Angew. Chem. Int. Ed., 2018, 57, 5848
RuCo@NC hybrids	28	31	Nat. Commun. 2017, 8, 14969
Ru-MoO_2	29	31	J. Mater. Chem. A, 2017, 5, 5475

Ru@CN-0.16	32	53	Energy Environ. Sci., 2018, 11 , 800
Ru@NG-4	40	76	Sustainable Energy Fuels, 2017, 1, 1028
RuO_2/N-C	40	44	ACS Sustainable Chem. Eng. 2018, 6, 11529
Ru_2Ni_2 SNs/C	40	23	Nano Energy, 2018, 47, 1
Ru ND/C	43	49	Chem.Commun., 2018, 54, 4613
CoRu@NC-2	45	66	Nanotechnology, 2018, 29,225403
Ru_2P@PNC/CC900	50	66	ACS Appl. Energy Mater. 2018, 1, 3143
Sr_2RuO_4	61	51	Nat. Commun., 2019, 10, 149
Anhydrous RuO_2@C	63	62	Nano Energy, 2019, 55, 49
RuPx@NPC	74	70	ChemSusChem, 2018, 11, 743
$Cu_{2-x}S$@Ru NPs	82	48	Small, 2017, 13, 1700052

Table6 Bader charge result.

Bader charge	Ru	W	N	O
Ru-W_2N/WO_2	0.67	0.93	-0.89	-1.06
W_2N/WO_2		0.91	-0.88	-1.03

1. G. Kresse and D. Joubert, Phys. Rev. B 1999, 59, 1758.

2. P.E. Blochl, Phys. Rev. B: Condens. Matter., 1994, 50, 17953-17979.

3. J. P. Perdew, K. Burke and M. Ernzerhof, Phys. Rev. Lett., 1996, 77, 3865-3868.

4. J. P. Perdew, M. Ernzerhof and K. Burke, J. Chem. Phys., 1996, 105, 9982-9985.

5. S. Grimme, J. Antony, S. Ehrlich and H. Krieg, J. Chem. Phys., 2010, 132, 154104-154123.

6. H. H. Li, Y. Wu, C. Li, Y. Y. Gong, L. Y. Niu, X. J. Liu, Q. Jiang, C. Q, Sun and S. Q. Xu, Appl. Catal. B: Environ., 2019, 251, 305–312.